

Scanning Electron Microscope-Energy Dispersive X-Ray (SEM-EDX) Study of Fe-C Catalyst from Iron Sand and Biochar for Advance Oxidation Process (AOPs)

Joko Pitoyo*, Siti Jamilatun**

*Department of Chemical Engineering, Faculty of Industrial Technology, Universitas Ahmad Dahlan, Jl. Jend. Ahmad Yani, Banguntapan, Bantul, Yogyakarta, Indonesia 55166
(joko2107054001@webmail.uad.ac.id, sitijamilatun@che.uad.ac.id)

‡Corresponding Author; Siti Jamilatun, Department of Chemical Engineering, Faculty of Industrial Technology, Universitas Ahmad Dahlan, Tel: +62 813-2915-7053, sitijamilatun@che.uad.ac.

Received: 02.09.2023 Accepted:05.10.2023

Abstract- Synthetic dyes are the primary water contaminants. Most synthetic dyes are thermally and chemically unreactive, highly poisonous, and non-biodegradable. Fenton is a clean technology that can oxidize hazardous, non-biodegradable organic pollutants into non-toxic inorganic species. This paper aims to characterize the Fe-C as a Fenton methods catalyst using SEM-EDX analysis. Fe-C catalyst synthesized through wet impregnation of Fe extracted from iron sand and bio-char product of sugarcane bagasse (SB), palm shell (PS), and empty fruit bunch (EFB) pyrolysis. Fe is obtained through the ultra-sonication process of a mixture of iron sand and concentrated HCL, while biochar is obtained from the pyrolysis process of PS, SB, and EFB at a temperature of 450 °C for 2 h. The catalyst was analyzed using SEM-EDX and then processed using Image J to determine its outer surface characteristics. The EDX analysis shows that Fe-CPS catalyst has the highest Fe content of 0.29 g of Fe per 5 g of catalyst, followed by Fe-CEFB and Fe-CSB with Fe content of 0.074 g and 0.077 g of Fe per 5 g of catalyst, respectively. The SEM analysis confirms that the Fe-CPS catalyst has the highest surface roughness, the widest pore distribution, and the highest mean pore size. These characteristics will increase the surface area of the catalyst thereby improving the adsorption ability of Fe₂O₃ and pollutants. The Fe-C system combines the adsorption capabilities of biochar with the oxidation performance of OH* through the activation of H₂O₂ by Fe₂O₃ attached to the biochar in the same process.

Keywords Synthetic dyes, Fenton, Biochar, SEM-EDX, Catalyst.

1. Introduction

The high population accompanied by increasing industrial and commercial activities causes a decrease in fossil fuel reserves, increases environmental problems, global warming, and worsens the quality of health [1, 2]. This energy crisis in the form of reduced fossil fuel, demands the invention of alternative energy resources to ensure the fulfillment of world energy needs [3, 4]. Biomass has been identified as a renewable, ecologically friendly, and sustainable energy source. [5, 6].

Biomass can be transformed into biofuels via thermochemical procedures like combustion, pyrolysis, and gasification. Pyrolysis is a thermal decomposition without oxygen or air [7–9]. Because of its versatility in making raw material choices, extended temperature operating range (300–600 °C), capability of operating under atmospheric pressure, and capacity to simultaneously produce three valuable products (solid, liquid, and gas), it is regarded as being superior to other thermo-chemical conversions [10–12]. Jamilatun et al. [13] carried out bagasse pyrolysis in a fixed bed reactor at 300–600°C using a sample grain size of 10–40 mesh and a heating rate of 10–12 °C/min. This process produces 42% liquid product which is dominated by

levoglucosan, 34% gas product which is dominated by CH₄, and 24% biochar with a surface area of 180.30 m²/g.

Biochar is a pyrolysis-derived solid. Biochar is a carbon-rich, porous substance that is frequently created by slowly pyrolyzing waste biomass [14, 15]. The pyrolysis procedure releases moisture and volatiles from the biomass while keeping the aromatic compounds and chemical functional groups, leaving behind a porous structure. Due to its advantageous properties, biochar can be used for a variety of purposes, including soil improvement, energy production, and pollution reduction. Biochar can increase the fertility of soil by improving nutrients and water retention. [16, 17]. In environmental remediation, it has also been used as a successful pollutant adsorbent [18]. Kong et al. [19] conducted microwave-assisted pyrolysis of oil palm shell using the frequency of 2.45 GHz, heating power 900 W resulting in biochar with a surface area of 410 m²/g and adsorption capacity of methylene blue of 20 mg/g.

On the other hand, in recent decades there has been a significant increase in water pollution, making it necessary to remove contaminants from industrial wastewater before releasing them into the environment [20]. The two main pollutants are synthetic dyes and heavy metals in water. Dyes are required in various industries, including wool, printing, leather textiles, paper, and cosmetics. Most synthetic dyes are thermally and chemically unreactive, highly poisonous, and non-biodegradable [21, 22]. Nearly 700,000 tons of dye are produced worldwide each year, which results in the commercial availability of nearly 100,000 dyes [23]. Various physiochemical methods have been studied for textile wastewater treatment, including coagulation [24], reverse osmosis [25], catalysis [26], adsorption [27], advanced oxidation process (AOPs) [28], and synchronized oxidation-adsorption (SOA) [29]. Fenton oxidation is one of the most efficient AOPs and has been used extensively to remove resistant organic contaminants. Fenton oxidation is a clean technology that can oxidize hazardous, non-biodegradable organic pollutants into non-toxic inorganic species.

Many studies have been conducted on the use of biochar for wastewater treatment [30, 31]. However, the use of a combination of biochar and the Fenton method for wastewater treatment through simultaneous adsorption and oxidation processes is still rarely studied, especially involving heterogeneous reactions between Fe²⁺ and H₂O₂. This study will provide new discourse related to AOPs, especially for processing synthetic dye waste. This paper studies the SEM-EDX analysis of the Fe-C catalyst from different sources of biomass waste, as a heterogeneous catalyst for the Fenton method which involves simultaneous adsorption and oxidation processes. This study can be a preliminary study to determine the performance of the catalyst in the Fenton method. Thus the conversion of biomass into biochar provides double advantages as a source of alternative green fuel for fossil fuel substitution through the pyrolysis process and as a heterogeneous catalyst in the Fenton method for wastewater treatment.

2. Materials and Methods

2.1. Materials

Iron sand was collected from Glagah Indah Beach Kulon Progo Yogyakarta. Iron sand is used as a source of Fe because it is abundant on Glagah Indah Beach, the southern coast of Java Island, Indonesia [32]. This iron sand has a high Fe content as can be seen in Table 1.

Table 1. Elemental composition of iron sand from Glagah Indah Beach.

Element	Mass,%
O	43.18
Na	0.92
Mg	1.43
Si	6.43
Ca	0.70
Ti	3.78
Fe	43.55

Palm shell (PS) and empty fruit bunch (EFB) were acquired from PT Perkebunan Nusantara (PTPN) V Riau. Sugarcane bagasse (SB) was provided by PT Madukismo Yogyakarta. These three biomass wastes were chosen because they are plantation crops which are quite abundant as can be seen in Figure 1. Before the next process, 1 kg sample is cleaned and chopped into small pieces, then soaked in NaOH 6%(w/v) for 24 h. The solid product was washed with water to get a neutral pH of (6-7) and then dried using an oven at 105 °C for 24 h. The dried sample is grounded and sieved to obtain a grain size of 10-40 mesh. The purpose of soaking in NaOH is believed to cleavage of lignin-carbohydrate connections, which increases porosity and internal and surface area of biochar [33].

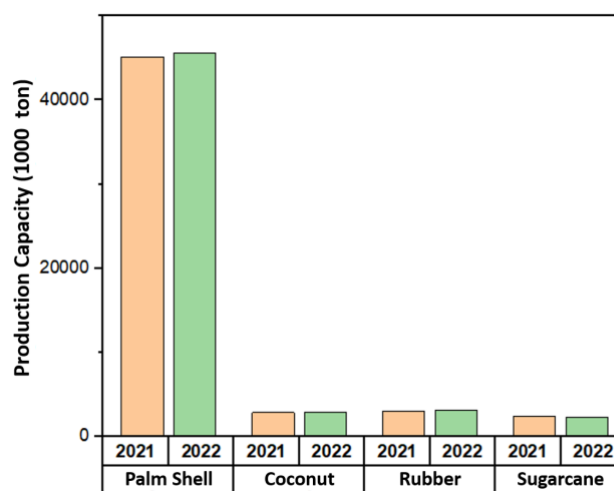


Fig. 1. Production capacity of main plantation crops in 2021 and 2022 [34].

2.2. Pyrolysis Experiment

A fixed bed reactor with an inner diameter of 400.00 mm, an outer diameter of 44.00 mm, and a height of 600.00 mm was used to conduct the pyrolysis process. The reactor had an electric heater made of nickel wire that was spirally coiled around the reactor's exterior. A thermocouple was used to measure the heating temperature, and a 0.5 kva TGDC regulator was used to control the heating rate. The pyrolysis process was conducted by inserting 1 kg of sample into the reactor. The sample was then heated at a heating rate of 10 °C /min to the temperature of 450 °C. After reaching the expected temperature, the heating was continued isothermally for 2h to obtain the biochar.

2.3. Purification of Iron Sand

A magnetic separator is used to separate magnetite from iron sand. The magnetite is sieved to obtain the mesh screen size of 100 mesh. 10 g of extracted magnetite were suspended in 54 mL of concentrated HCl (37%) and left for ultra-sonication at various irradiation times using a sonicator bath at ambient temperature. This process uses a frequency of 30 kHz. To produce the FeCl₂ and FeCl₃ solutions, 0.8 µm filter paper was used to filter the suspension solution. The filtrate was gradually added ±50 mL of 6.5 M NH₄OH solution until a black precipitate (Fe₃O₄), as a starting precursor for synthesizing Fe-C catalyst [35], was developed. The precipitate was repeatedly rinsed with ethanol and distilled water until a pH of neutral was obtained. The solution was centrifuged to separate the precipitate and then dried in an oven at 60°C for ± 12 h, and then collected using a magnet.

2.4. Preparation of Fe-C Catalyst

The iron nanoparticles obtained were dissolved in 10 ml of isopropyl alcohol. The solution is then mixed with 5 g of sample-activated carbon, stirred for 1 h with an ultrasonicator, and dried for 24 h until the isopropyl alcohol evaporates. The mixture was calcined at 300°C for 3 h. Isopropyl alcohol is a nonaqueous medium to synthesize Fe-C catalyst. During the ultra-sonication process several active species are formed from the ultrasonolysis of isopropyl alcohol, among these species, solvated electrons are strong reduction radicals that can reduce Fe₃O₄ to Fe atoms [36], [37]. The Fe atoms formed will quickly oxidized resulting in the formation of Fe₂O₃ nanoparticles on the biochar surface as activators of H₂O₂ [38]. Meanwhile, the calcination process aims to obtain a catalyst with a large pore size, large surface area, and high mechanical and thermal resistance [39]. The reason for using low temperatures, 300°C is more isolated Fe₂O are preserved at low calcination temperatures [40].

2.5. Characterization of Fe-C Catalyst

A scanning electron microscope-energy disperse X-ray (SEM-EDX) using a JSM-6510 instrument was performed for catalyst characterization to determine the surface morphology (porosity, roughness, and shape) of the catalyst

and the composition of the element. For acquiring images and sample composition data with an SEM tool, the sample was placed and attached to the top of the SEM specimen holder using carbon double type with a cross-section pointing vertically upwards or towards the objective lens. So that the matrix layers of the material are visible. This double tip is made of conductive carbon material on both sides which function to deliver all the electrons that enter the sample out through grounding. The sample chamber was vacuumed to 10⁻⁶ torr to guarantee that the SEM column was free of air molecules. SEM analysis was operated at an accelerating voltage of 15kV, a working distance (WD) of 6 mm, a spot size (SS) of 40, and magnificient of 500, 1000, and 2500.

2.6. SEM-EDX Data Analysis

SEM-EDX analysis provides high-resolution images of the sample surface along with details on the chemical composition and elemental distribution [41, 42]. The resulting image can be further processed using specific software to determine the distribution of pores, porosity, and surface roughness. There are several open-source software programs for image analysis, including Image J, Qupath, Ilastik, Orbit, Cytomine, and Icy. Among this software, Image J is the most widely used because of its simple-to-use architecture, recordable macro language, and extendable plug-in system [43]. In this analysis, Image J software was utilized to calculate the pore distribution on the catalyst surface, porosity, and surface roughness. The steps of the image processing and analysis can be seen in Figure 2.

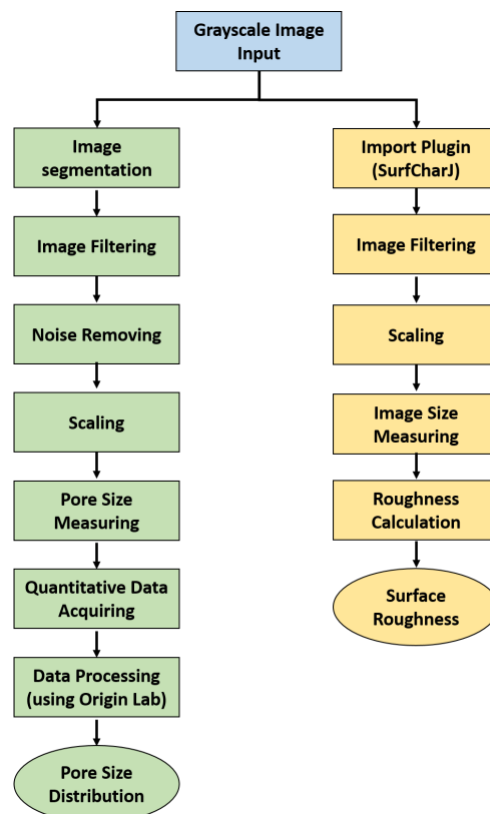


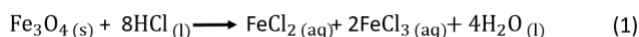
Fig. 2. Image processing and analyzing algorithms

3. Result and Discussion

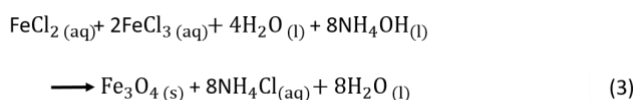
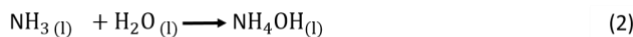
3.1. Catalyst Preparation

Preparation of Fe-C catalyst includes pyrolysis of biomass, iron sand purification, and wet impregnation of catalyst. In the pyrolysis process, palm shell, sugarcane bagasse, and empty fruit bunches are used because they are agricultural waste with abundant quantities and low prices which are the main requirements as raw materials. Pyrolysis is carried out at a temperature of 450°C because at this temperature the volatile materials, including cellulose and hemicellulose, are completely decomposed and leave lignin residue as the main constituent of biochar. The hemicellulose decomposition occurs between the temperature of 250 and 350°C, and cellulose at 325 to 400°C, and the decomposition of lignin occurs at 300-550°C [44, 45]. A higher pyrolysis temperature will cause gasification to occur which will reduce the amount of biochar produced. A slow pyrolysis (heating rate of 10°C /min) is used because slow pyrolysis is preferred for the formation of biochar.

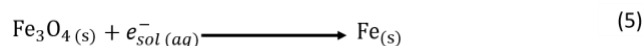
Iron sand is used as a source of Fe because it has abundant amounts and high magnetite (Fe₃O₄) content. In the purification process, magnetite is reacted with concentrated HCL to produce FeCl₂ and FeCl₃ through the following reaction:



Further reaction with NH₄OH will produce a black precipitate Fe₃O₄. The occurring reaction is:



Fe₂O₃ has recently received a lot of attention for wastewater purification due to its benefits in terms of chemical resistance, low processing costs, large specific surface area, and satisfactory visible-light response [46]. The fabrication of Fe₂O₃ from magnetite (Fe₃O₄) can be carried out using gamma-ray irradiation [37], hydrothermal method, chemical precipitation method, sol-gel method, anodization, electrochemical method [46], thermal decomposition methods, and micro fluidized bed reaction [47]. In this research, the ultrasonication method was used, which is part of the thermal decomposition method. The suggested reaction is as follows.



During the ultrasonication process several active species are formed from the sonolysis of isopropyl alcohol, among these species, solvated electrons are strong reduction that can reduce Fe₃O₄ to Fe [36, 37]. The Fe adsorbed on the surface of the catalyst will quickly be oxidized resulting in the formation of Fe₂O₃ nanoparticle.

3.2. SEM-EDX Analysis

The basic principle of SEM is to bombard and scan the sample's surface with a focused electron beam fired from an "electron gun" to stimulate different physical signals in the sample, including backscattered electrons, secondary electrons, absorbed electrons, and projected electrons. The signal-collecting system detects, amplifies, and processes these physical signals before delivering the scanned images of various topographic aspects of the sample surface to the image display system [41]. The ability to design adsorbents for improved or selective removal of particular pollutants depends on understanding the pore structure of adsorbents, including pore size and shape, pore surface chemistry, and pore volume [48]. Based on the International Union of Pure and Applied Chemistry (IUPAC), pore size is classified into micropore (<2 nm), mesopore (2-50 nm), and macropore (>50 nm) [49]. These existing pores in the biochar are due to the decomposition of volatile matter, cellulose, hemicellulose, and lignin along the pyrolysis. Within the material's particles, the pyrolysis process results in the opening of channels, thus giving a rough surface texture [50]. The morphology of the catalyst shows a differential porosity developed and the formation of the surface with different sizes of pores separated by walls; this porosity increases the specific surface, and consequently, improves the capacity of the catalyst [51].

The SEM-EDX of Fe-C has been presented in Figure 3. The figure indicated that the pyrolysis process results catalyst with porous carbon surfaces that are exhibited in macropore structure. Thus, the outer surface of the catalyst is observed to be in the form of a large slit pore. This occurs as a result of SEM analysis's restriction to macropore size. As previously stated, the pyrolysis process results in the opening of channels, the presence of large slit pores on the outer surface of the catalyst is expected to be an indication of the easy opening of channels in the catalyst which causes more pores to form inner the catalyst. The high porosity will increase the specific surface area thereby increasing the possibility of Fe³⁺ ions and synthetic dyes to be adsorbed on the catalyst surface consequently improving the oxidation process and adsorption capacity in heterogeneous Fenton oxidation.

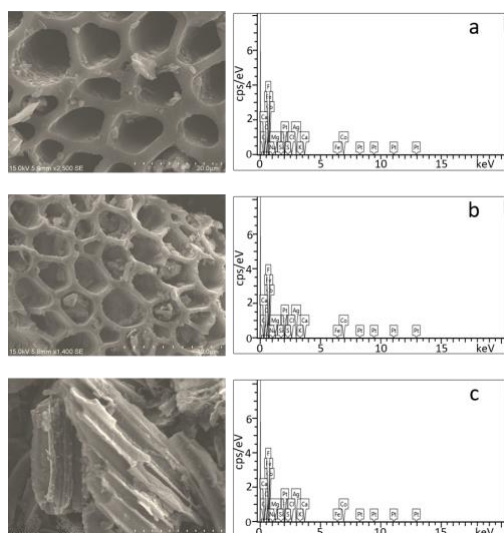


Fig. 3. SEM-EDX of a) Fe-CSB, b) Fe-CPS, and c) Fe-CEFB

The qualitative examination by energy disperse X-ray (EDX) results indicates that carbon dominates the whole sample, which confirms the catalyst's organic nature [27]. We further note the presence of considerable Fe on the catalyst surface which confirms the impregnation process success, especially for PS catalyst which supported the Fenton method' use of them as a catalyst [52] or synchronized oxidation-adsorption (SOA) process. There are many elements other than Fe in significant amounts detected in EDX analysis, namely O, Mg, and Co. The O element detected is an oxide. This element exists in large quantities. This element comes from several metallic oxides such as Na₂O, MgO, SiO₂, Fe₂O₃, P₂O₅, CaO, and K₂O. The element magnesium (Mg) is the third largest element after carbon and oxide, this element can inhibit the decomposition of H₂O₂ into OH* radicals in alkaline conditions (pH 9) [53]. Another element with significant amounts detected was cobalt (Co). This element is useful for the Fenton method. Cobalt can activate H₂O₂ to become superoxide which plays a role in the degradation of dye waste [54].

Table 2. Elemental composition in mass% of Fe-C catalyst

Elements	Mass%		
	Fe-CSB	Fe-CPS	Fe-CEFB
C	46.07	40.12	32.71
O	44.31	29.31	22.01
F	0	0	0
Na	0	0	0
Mg	4.81	9.63	6.4
Si	0.08	0.48	0.09
P	0	0	0
S	0.11	0	0.19
Cl	0.14	0	0.36
K	0.23	0.89	31.67
Ca	0.28	5.6	2.9
Fe	1.48	5.83	1.55

Co	2.07	8.14	2.13
Ag	0.41	0	0

3.3. Surface Characteristic

Figure 4 shows a 3D surface plot of the catalyst surface. The height of the image interprets the luminance of the image. The blue sea color shows the existence of pores on the catalyst surface. The figure reveals that Fe-CSB and Fe-CPS catalysts have more pores than Fe-CEFB.

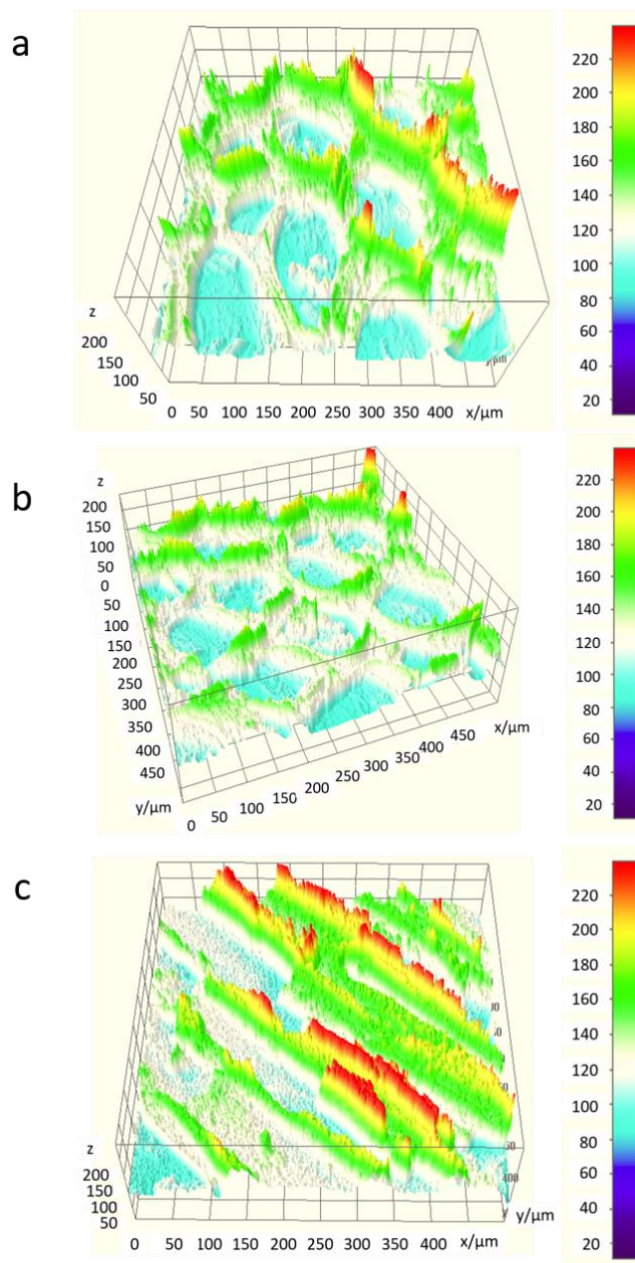


Fig. 4. 3D surface plot of a) Fe-CSB, b) Fe-CPS, and c) Fe-CEFB

The catalyst's surface plot and computation of its roughness are shown in Figure 5. The surface roughness represents the degree of heterogeneity. The higher the heterogeneity, the larger the roughness and irregularity. The

pore surface's high roughness creates a greater specific surface area for adsorption, increasing the adsorption capacity. The roughness characteristic of the catalyst surface was indicated by the root mean square of roughness (Rq) and average of roughness (Ra). The higher the Rq and Ra value, the rougher the catalyst surface. Figure 5 reveals that Fe-CPS has the highest roughness with an Rq value of 126.468, followed by Fe-CEFB, and then Fe-CSB with an Rq value of 123.040 and 114.934, respectively.

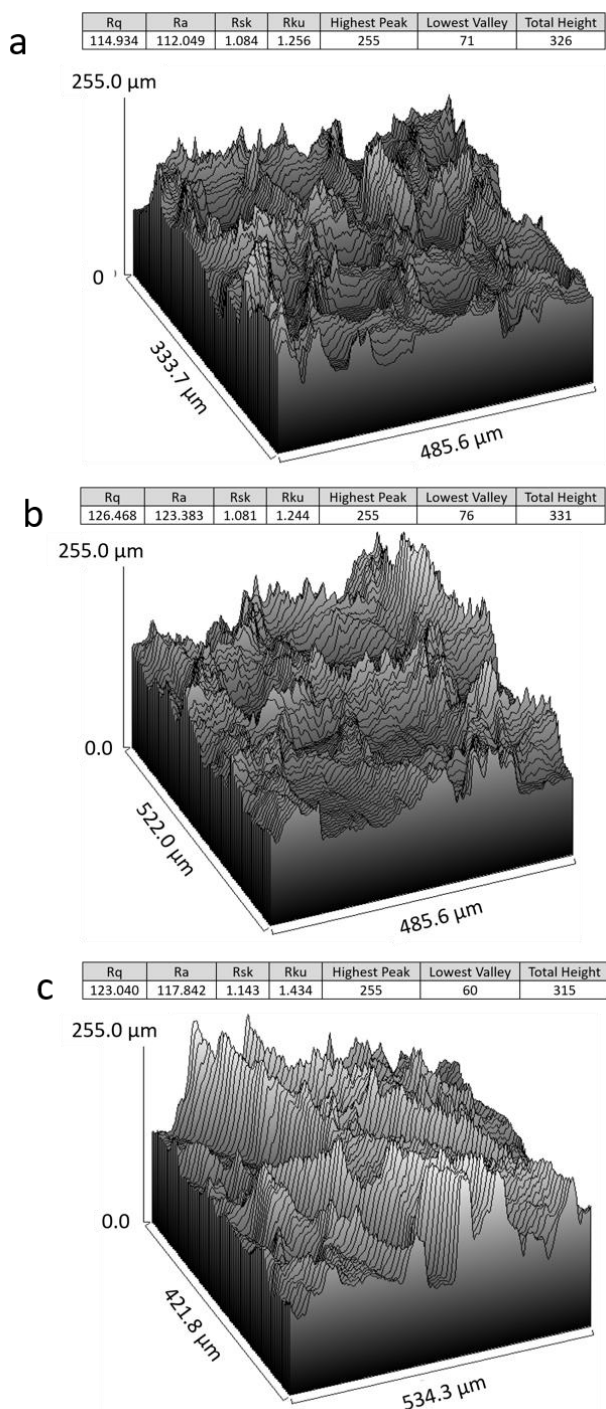


Fig. 5. Surface plot and roughness calculation of a) Fe-CSB, b) Fe-CPS, and c) Fe-CEFB

3.4. Pore Size Distribution

Adsorption is a surface reaction, hence having a large surface area is frequently seen as a key factor in enhancing adsorption capability. Pores of various sizes contribute to the surface area of such porous catalysts. Their accessibility by dye molecules may be influenced by the size and configuration of the pores. Additionally, dye's diffusion into such pores may be impacted [55].

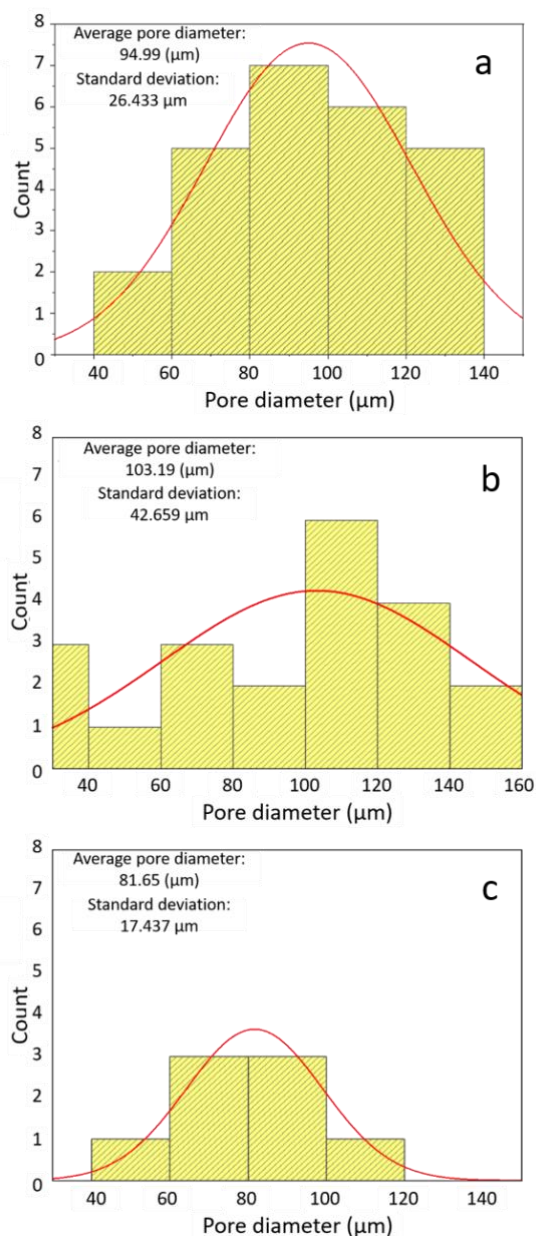


Fig. 6. Pore size distribution of a) Fe-CSB, b) Fe-CPS, and c) Fe-CEFB

Catalysts with a microporous structure have a large surface area, but have limitations including being prone to pore closure, and coking, and are not suitable for adsorbing waste with relatively large particle sizes such as methylene blue (1,447 nm) [49]. Catalysts with a mesoporous structure, although they have a smaller surface area, have a small

adsorption capacity, but the adsorption occurs at a greater rate. Meanwhile, catalysts with a macropore structure have a low adsorption capacity [41]. Catalysts with a wide pore distribution provide a great possibility to adsorb pollutants with large variations in size. Also, the wide distribution of pore size indicates the high roughness surface catalyst, consequently increasing the surface area. Meanwhile, the high mean pore diameter on the outer surface of the catalyst is expected to be an indication of the easy opening of channels in the catalyst during pyrolysis which causes more pores to form inner the catalyst.

The histogram of the pore size distribution (PSD) and the normal distribution curve of the catalyst are shown in Figure 6. The mean pore diameter and the standard deviation of Fe-CSB, Fe-CPS, and Fe-CEFB are 94.99, 103.19, 81.65, and 26.43, 42.66, and 17.43 μm , respectively. Fe-CPS has a higher mean pore diameter and wider distribution (standard deviation) than others, this is possibly due to the self-extrusion of volatile matters from the inside the palm shell, leaving behind a high lignin complex which has a complex structure that is not completely decomposed at a temperature of 450°C. The high mean pore diameter and the wide pore distribution on the outer surface of the Fe-CPS catalyst are expected to have high porosity and high heterogeneity (surface roughness and irregularity) thereby increasing the surface area of the catalyst which results in high adsorption capacity.

4. Conclusion

Fe-C catalyst was successfully obtained from SB, PS, and EFB biochar. The EDX and SEM analysis shows that Fe-CPS catalyst has the Fe content of 5.83 %, root mean square of roughness (Rq) of 126.46, mean pore diameter of 103.19 μm , and standard deviation of 42.659 μm , Fe-CEFB with Fe content of 1.48 %, root mean square of roughness (Rq) of 114.934, mean pore diameter of 94.99 μm , and standard deviation of 26.433 μm , and Fe-CSB with Fe content of 1.55 %, root mean square of roughness (Rq) of 123.040, mean pore diameter of 81.65 μm , and standard deviation of 17.437 μm respectively. The result confirms that the Fe-CPS catalyst has the highest value of Fe content, surface roughness, mean pore size and pore size distribution. The high Fe content will increase the activation of H_2O_2 in the Fenton method. High values of Rq, mean pore diameter and standard deviation are expected to increase catalyst porosity thereby increasing the surface area. These properties can improve the application of the Fenton method as an advanced oxidation process (AOPs). The insights from this study will help to design heterogeneous Fe-C catalysts with an appropriate characteristics and use SEM-EDX analysis as a preliminary study to determine the performance of the different catalysts.

Acknowledgments

The author is very appreciative of the research funding support provided through the "Directorate of Research, Technology, and Community Service from the Ministry of Education, Culture, Research, and Technology" under the National Competitive Basic Research (PDKN) scheme, for

the Fiscal Year 2023, Number 006/PDKN/LPPM UAD/IV/2023.

References

- [1] I. Ali, H. Bahaitham, and R. Naibulharam, "A comprehensive kinetics study of coconut shell waste pyrolysis," *Bioresour. Technol.*, vol. 235, pp. 1–11, 2017, doi: 10.1016/j.biortech.2017.03.089.
- [2] A. Hassan, S. Zafar Ilyas, H. Mufti, "Review of the renewable energy status and prospects in Pakistan" *International Journal of Smart Grid - ijSmartGrid*, vol. 5, no.4,2021, doi:10.20508/ijsmartgrid.v5i4.220. g174.
- [3] J. O. Ighalo and A. G. Adeniyi, "Factor effects and interactions in steam reforming of biomass bio-oil," *Chem. Pap.*, vol. 74, no. 5, pp. 1459–1470, 2020, doi: 10.1007/s11696-019-00996-3.
- [4] B. Hangun, O. Eyecioglu, and M. Beken, "Investigating the Energy Production Trends of Countries and Its Relationship Between Economic Development," 11th IEEE Int. Conf. Renew. Energy Res. Appl. ICRERA 2022, pp. 597–600, 18-21 September 2022.
- [5] I. M. Rajendra, I. N. S. Winaya, A. Ghurri, and I. K. G. Wirawan, "Pyrolysis study of coconut leaf's biomass using thermogravimetric analysis," *IOP Conf. Ser. Mater. Sci. Eng.*, vol. 539, no. 1, 2019, doi: 10.1088/1757-899X/539/1/012017.
- [6] A. Ziya Aktas, "A Review and comparison of renewable energy strategies or policies of some countries," 2015 Int. Conf. Renew. Energy Res. Appl. ICRERA 2015, vol. 5, pp. 636–643, 22-25 November 2015.
- [7] J. Pitoyo, T. Eka, and S. Jamilatun, "Bio-oil from Oil Palm Shell Pyrolysis as Renewable Energy: A Review," *Chemica*, vol. 9, no. 2, pp. 67–79, 2022. doi: 10.26555/chemica.v9i2.22355
- [8] R. E. Guedes, A. S. Luna, and A. R. Torres, "Operating parameters for bio-oil production in biomass pyrolysis: A review," *J. Anal. Appl. Pyrolysis*, vol. 129, no. November 2017, pp. 134–149, 2018, doi: 10.1016/j.jaap.2017.11.019.
- [9] J. Pitoyo, S. Jamilatun, and M. Setyawan, "Technical , Economic , and Environmental Review of Waste to Energy Technologies from Municipal Solid Waste," *J. I. Lingkungan*, vol. 21, no. 3, pp. 576–588, 2023, doi: 10.14710/jil.21.3.576-588.
- [10] L. M. Terry, C. Li, J. J. Chew, A. aqsha, B. S. how, A. C. M. Loy, B. L. F. Chin, D. S. Khaerudini, N. Hamid, G. guan, and J. Sunarso, "Bio-oil production from pyrolysis of oil palm biomass and the upgrading technologies: A review," *Carbon Resour. Convers.*, vol. 4, no. October, pp. 239–250, 2021, doi: 10.1016/j.crcon.2021.10.002.
- [11] S. Jamilatun, Budhijanto, Rochmadi, A. Yuliestyan, and A. Budiman, "Valuable chemicals derived from

- pyrolysis liquid products of spirulina platensis residue,” *Indones. J. Chem.*, vol. 19, no. 3, pp. 703–711, 2019, doi: 10.22146/ijc.38532.
- [12] S. Hosokai, K. Matsuoka, K. Kuramoto, and Y. Suzuki, “Estimation of thermodynamic properties of liquid fuel from biomass pyrolysis,” *3rd Int. Conf. Renew. Energy Res. Appl. ICRERA 2014*, vol. 5, pp. 728–731, 19-22 Oktober 2014.
- [13] S. Jamilatun, J. Pitoyo, S. Amelia, A. Ma, D. C. Hakika, and I. Mufandi, “Experimental Study on The Characterization of Pyrolysis Products from Bagasse (*Saccharum Officinarum* L.): Bio-oil , Biochar , and Gas Products,” *Indonesian Journal of Science & Technology*, vol. 7, pp. 565–582, 2022. doi: 10.17509/ijost.v7i3.51566
- [14] E. M. Valdés-Rodríguez, D. I. Mendoza-Castillo, H. E. Reynel-Ávila, I. A. Aguayo-Villarreal, and A. Bonilla-Petriciolet, “Activated carbon manufacturing via alternative Mexican lignocellulosic biomass and their application in water treatment: Preparation conditions, surface chemistry analysis and heavy metal adsorption properties,” *Chem. Eng. Res. Des.*, vol. 187, pp. 9–26, 2022, doi: 10.1016/j.cherd.2022.08.039.
- [15] A. Peter, B. Chabot and E. Loranger, "Enhancing Surface Properties of Softwood Biochar by Ultrasound Assisted Slow Pyrolysis," 2019 IEEE International Ultrasonics Symposium (IUS), Glasgow, UK, 2019, pp. 2477-2480, 06-09 October 2019.
- [16] L. Wang, H. Lei, Q. Bu, S. Ren, Y. wei, L. Zhu, X. zhang, Y. Liu, G. Ydavalli, J. Lee, S. Chen, and J. Tang, “Aromatic hydrocarbons production from ex situ catalysis of pyrolysis vapor over Zinc modified ZSM-5 in a packed-bed catalysis coupled with microwave pyrolysis reactor,” *Fuel*, vol. 129, pp. 78–85, 2014, doi: 10.1016/j.fuel.2014.03.052.
- [17] S. Li, H. Jin, L. Gao, X. Zhang, and X. Ji, “Techno-economic performance and cost reduction potential for the substitute/synthetic natural gas and power cogeneration plant with CO₂ capture,” *Energy Convers. Manag.*, vol. 85, pp. 875–887, 2014, doi: 10.1016/j.enconman.2013.12.071.
- [18] X. Liu, F. Shen, R. L. Smith, and X. Qi, “Black liquor-derived calcium-activated biochar for recovery of phosphate from aqueous solutions,” *Bioresour. Technol.*, vol. 294, no. 38, p. 122198, 2019, doi: 10.1016/j.biortech.2019.122198.
- [19] S. H. Kong, S.S. Lam, P. Yek, R. K. Liew, N. L. Ma, M. Osman, and W. Chung, “Self-purging microwave pyrolysis: An innovative approach to convert oil palm shell into carbon-rich biochar for methylene blue adsorption,” *J. Chem. Technol. Biotechnol.*, vol. 94, Nov. 2018, doi: 10.1002/jctb.5884.
- [20] P. Rai, R. K. Gautam, S. Banerjee, V. Rawat, and M. C. Chattopadhyaya, “Synthesis and characterization of a novel SnFe₂O₄-activated carbon magnetic nanocomposite and its effectiveness in the removal of crystal violet from aqueous solution,” *J. Environ. Chem. Eng.*, vol. 3, no. 4, pp. 2281–2291, 2015, doi: 10.1016/j.jece.2015.08.017.
- [21] O. León, A. M. Bonilla, D. Soto, D. Perez, M. Rangel, M. Colina, and M. F. Garcia, “Removal of anionic and cationic dyes with bioadsorbent oxidized chitosans,” *Carbohydr. Polym.*, vol. 194, no. March, pp. 375–383, 2018, doi: 10.1016/j.carbpol.2018.04.072.
- [22] Y. Lijun and D. Qunwei, "The Reactive Light Yellow Dye Wastewater Treatment by Sewage Sludge-Based Activated Carbon," 2011 International Conference on Computer Distributed Control and Intelligent Environmental Monitoring, Changsha, China, 2011, pp. 646-649, 19-20 February 2011.
- [23] R. N. Bharagava and P. Chowdhary, “Emerging and eco-friendly approaches for waste management,” *Emerg. Eco-Friendly Approaches Waste Manag.*, no. March, pp. 1–435, 2018, doi: 10.1007/978-981-10-8669-4.
- [24] J. Dotto, M. R. Fagundes-Klen, M. T. Veit, S. M. Palácio, and R. Bergamasco, “Performance of different coagulants in the coagulation/flocculation process of textile wastewater,” *J. Clean. Prod.*, vol. 208, pp. 656–665, 2019, doi: 10.1016/j.jclepro.2018.10.112.
- [25] Y. J. Tan, L. J. Sun, B. T. Li, X. H. Zhao, T. Yu, N. Ikuno, K. Ishii, and H. Y. Hu, “Fouling characteristics and fouling control of reverse osmosis membranes for desalination of dyeing wastewater with high chemical oxygen demand,” *Desalination*, vol. 419, no. June, pp. 1–7, 2017, doi: 10.1016/j.desal.2017.04.029.
- [26] M. Farsi and A. Nezamzadeh-Ejehieh, “A coupled Cobalt(II) oxide-Silver Tungstate nano-photocatalyst: Moderate characterization and evaluation of the photocatalysis kinetics towards methylene blue in aqueous solution,” *Polyhedron*, vol. 219, p. 115823, 2022, doi: 10.1016/j.poly.2022.115823.
- [27] M. H. Nabih, M. Hajam, H. Boulrika, Z. Tiki, S. B. Tahar, N. I. Kandri, and A. Zerouale, “Materials Today : Proceedings Preparation and characterization of activated carbons from cardoon “ *Cynara Cardunculus* ” waste: Application to the adsorption of synthetic organic dyes,” *Mater. Today Proc.*, vol. 72, pp. 3369–3379, 2023, doi: 10.1016/j.matpr.2022.07.414.
- [28] G. Dong, B. Chen, B. Liu, L. J. Hounjet, Y. Cao, S. R. Stoyanov, M. Yang, and B. Zhang, “Advanced oxidation processes in microreactors for water and wastewater treatment: Development, challenges, and opportunities,” *Water Res.*, vol. 211, p. 118047, 2022, doi: 10.1016/j.watres.2022.118047.
- [29] Q. Jin, Y. Zhan, D. Tao, T. Wang, J. S. Khim, and Y. He, “Removing emerging e-waste pollutant DTFPB by synchronized oxidation-adsorption Fenton technology,” *J. Hazard. Mater.*, vol. 445, no. November 2022, p. 130587, 2023, doi: 10.1016/j.jhazmat.2022.130587.

- [30] M. M. Mian, G. Liu, B. Yousaf, B. Fu, H. Ullah, M. U. Ali, Q. Abbas, M. Mujtaba, A. Mehr, and L. Ruijia, "Simultaneous functionalization and magnetization of biochar via NH₃ ambient pyrolysis for efficient removal of Cr (VI)," *Chemosphere*, vol. 208, pp. 712–721, 2018, doi: 10.1016/j.chemosphere.2018.06.021.
- [31] R. K. Liew, C. Chai, P. Yek, X. Phang, M. Chong, W. L. Nam, M. H. Su, W. H. Lam, N. Y. Ma, and S. S. lam, "Innovative production of highly porous carbon for industrial effluent remediation via microwave vacuum pyrolysis plus sodium-potassium hydroxide mixture activation," *J. Clean. Prod.*, vol. 208, no. 2019, pp. 1436–1445, 2019, doi: 10.1016/j.jclepro.2018.10.214.
- [32] N. R. Ardiani, S. Setianto, B. Santosa, B. M. Wibawa, C. Panatarani, and I. Made Joni, "Quantitative analysis of iron sand mineral content from the south coast of cidaun, west Java using rietveld refinement method," *AIP Conf. Proc.*, vol. 2219, no. May, 2020, doi: 10.1063/5.0003018.
- [33] Y. Zheng, J. Zhao, F. Xu, and Y. Li, "Pretreatment of lignocellulosic biomass for enhanced biogas production," *Prog. Energy Combust. Sci.*, vol. 42, no. 1, pp. 35–53, 2014, doi: 10.1016/j.pecs.2014.01.001.
- [34] BPS-Statistics Indonesia, *Statistics Yearbook of Indonesia 2023*, Catalog: 1101001. BPS-Statistics Indonesia Press, 2023, pp. 318-319.
- [35] X. Peng and W. Luo, "Synthesis of Fe (OH) 3/g-C₃N₄ catalyst by a simple two-step method and application in organic pollutants degradation," *IOP Conf. Ser. Earth Environ. Sci.*, vol. 300, no. 3, 2019, doi: 10.1088/1755-1315/300/3/032101.
- [36] M. Anbar and I. Pecht, "The Sonolytic Decomposition of Organic Solutes in Dilute Aqueous Solutions. II. The Sonolysis of Isopropyl Alcohol," *J. Phys. Chem.*, vol. 68, no. 6, pp. 1462–1465, Jun. 1964, doi: 10.1021/j100788a032.
- [37] J. Du and H. Liu, "Preparation of superparamagnetic γ -Fe₂O₃ nanoparticles in nonaqueous medium by γ -irradiation," *J. Magn. Magn. Mater.*, vol. 302, no. 1, pp. 263–266, 2006, doi: 10.1016/j.jmmm.2005.09.016.
- [38] Q. Tao, J. Bi, X. Huang, R. Wei, T. Wang, Y. Zhou, and H. Hao, "Fabrication, application, optimization and working mechanism of Fe₂O₃ and its composites for contaminants elimination from wastewater," *Chemosphere*, vol. 263, p. 127889, 2021, doi: 10.1016/j.chemosphere.2020.127889.
- [39] J. A. Zazo, A. F. Fraile, A. Rey, A. Bahamonde, J. A. Casas, and J. J. Rodriguez, "Optimizing calcination temperature of Fe/activated carbon catalysts for CWPO," *Catal. Today*, vol. 143, no. 3–4, pp. 341–346, 2009, doi: 10.1016/j.cattod.2009.01.032.
- [40] Q. Liu, C. Bian, Y. Jin, L. Pang, Z. Chen, and T. Li, "Influence of calcination temperature on the evolution of Fe species over Fe-SSZ-13 catalyst for the NH₃-SCR of NO," *Catal. Today*, vol. 388–389, no. June 2020, pp. 158–167, 2022, doi: 10.1016/j.cattod.2020.06.085.
- [41] D. Liu, F. Qiu, N. Liu, Y. Cai, Y. Guo, B. Zhao, and B. Qiu, "Pore structure characterization and its significance for gas adsorption in coals: A comprehensive review," *Unconv. Resour.*, vol. 2, no. September, pp. 139–157, 2022, doi: 10.1016/j.unres.2022.10.002.
- [42] A. Lee, B. Zee and F. J. Foo, "Metallic Trace Contaminant Detection Using SEM/EDX," 2019 IEEE 26th International Symposium on Physical and Failure Analysis of Integrated Circuits (IPFA), Hangzhou, China, 2019, pp. 1-4, 02-05 July 2019.
- [43] T. Ferreira and W. Rasband, "ImageJ User Guide User Guide ImageJ," *Image J user Guid.*, vol. 1.46r, 2012, doi: 10.1038/nmeth.2019.
- [44] H. Yang, R. Yan, H. Chen, D. H. Lee, and C. Zheng, "Characteristics of hemicellulose, cellulose and lignin pyrolysis," *Fuel*, vol. 86, no. 12–13, pp. 1781–1788, 2007, doi: 10.1016/j.fuel.2006.12.013.
- [45] T. Aysu, M. M. Maroto-Valer, and A. Sanna, "Ceria promoted deoxygenation and denitrogenation of *Thalassiosira weissflogii* and its model compounds by catalytic in-situ pyrolysis," *Bioresour. Technol.*, vol. 208, pp. 140–148, 2016, doi: 10.1016/j.biortech.2016.02.050.
- [46] Y. Chen, L. Wei, X. Zhao, and J. Julson, "Modification, application and reaction mechanisms of nano-sized iron sulfide particles for pollutant removal from soil and water: A review," *Chem. Eng. J.*, vol. 362, no. December 2018, pp. 144–159, 2019, doi: 10.1016/j.cej.2018.12.175.
- [47] K. He, Z. Zheng, and Z. Chen, "Multistep reduction kinetics of Fe₃O₄ to Fe with CO in a micro fluidized bed reaction analyzer," *Powder Technol.*, vol. 360, pp. 1227–1236, 2020, doi: 10.1016/j.powtec.2019.10.094.
- [48] C. L. Mangun, M. A. Daley, R. D. Braatz, and J. Economy, "Effect of pore size on adsorption of hydrocarbons in phenolic-based activated carbon fibers," *Carbon N. Y.*, vol. 36, no. 1–2, pp. 123–129, 1998, doi: 10.1016/s0008-6223(97)00169-3.
- [49] J. O. Ighalo, K. O. Iwuozor, C. A. Igwegbe, and A. G. Adeniyi, "Verification of pore size effect on aqueous-phase adsorption kinetics: A case study of methylene blue," *Colloids Surfaces A Physicochem. Eng. Asp.*, vol. 626, no. July, p. 127119, 2021, doi: 10.1016/j.colsurfa.2021.127119.
- [50] F. Rahmawati, A. Ridassepri, Chairunnisa, A. T. Wijayanta, K. Nakabayashi, J. Miyawaki, and T. Miyazaki, "Carbon from bagasse activated with water vapor and its adsorption performance for methylene blue," *Appl. Sci.*, vol. 11, no. 2, pp. 1–16, 2021, doi: 10.3390/app11020678.
- [51] Y. Raji, A. Nadi, I. Mechnou, M. Saadouni, and O. Cherkaoui, "Diamond & Related Materials High

- adsorption capacities of crystal violet dye by low-cost activated carbon prepared from Moroccan *Moringa oleifera* wastes: Characterization, adsorption and mechanism study,” *Diam. Relat. Mater.*, vol. 135, no. March, p. 109834, 2023, doi: 10.1016/j.diamond.2023.109834.
- [52] Y. Pandey, A. Verma, and A. Pal, “Abatement of paraquat contaminated water using solar assisted heterogeneous photo-Fenton like treatment with iron-containing industrial wastes as catalysts,” *J. Environ. Manage.*, vol. 325, no. PB, p. 116550, 2023, doi: 10.1016/j.jenvman.2022.116550.
- [53] J. Abbot and D. G. Brown, “Stabilization of iron-catalysed hydrogen peroxide decomposition by magnesium,” *Can. J. Chem.*, vol. 68, no. 9, pp. 1537–1543, 1990, doi: 10.1139/v90-237.
- [54] L. V. Lombardo Lupano, J. M. Lázaro Martínez, L. L. Piehl, E. Rubin De Celis, and V. Campo Dall’Orto, “Activation of H₂O₂ and superoxide production using a novel cobalt complex based on a polyampholyte,” *Appl. Catal. A Gen.*, vol. 467, pp. 342–354, 2013, doi: 10.1016/j.apcata.2013.08.002.
- [55] P. Suresh Kumar, L. Korving, K. J. Keesman, M. C. M. van Loosdrecht, and G. J. Witkamp, “Effect of pore size distribution and particle size of porous metal oxides on phosphate adsorption capacity and kinetics,” *Chem. Eng. J.*, vol. 358, no. July 2018, pp. 160–169, 2019, doi: 10.1016/j.cej.2018.09.202.